

Upconversion red light emission and luminescence thermometry of $\text{Gd}_2\text{O}_3:\text{Er}^{3+}$ @ $\text{Gd}_2\text{O}_3:\text{Yb}^{3+}$ core-shell nanofibers synthesized via electrospinning

Z. Liu^{a,*}, R. X. Wang^a, K. W. Sun^b, X. C. Ling^b, J. W. Sun^b, D. H. Chen^c

^a*School of Science, Jinling Institute of Technology, Nanjing 211168, China*

^b*College of International Education, Jinling Institute of Technology, Nanjing 211168, China*

^c*State Key Laboratory of Optoelectronic Materials and Technologies, School of Electronics and Information technology, Sun Yat-sen University, Guangzhou 510275, China*

$\text{Gd}_2\text{O}_3:\text{Er}^{3+}$ @ $\text{Gd}_2\text{O}_3:\text{Yb}^{3+}$ core-shell nanofibers with cubic phase were successfully fabricated by electrospinning method. The structural, morphological properties were investigated by X-Ray diffraction, scanning electron microscopy. Under 980 nm excitation, the upconversion photoluminescence in visible light exhibits strong red emitting band with obvious splitting peaks resulted from stark splitting of energy level. The visible emissions are sensitive to temperature in the range of 303-543 K. The red emission displays quenching with elevation of temperature. The activation energy for thermal quenching is equal to 0.1408 eV. The temperature dependent multi-peaks of red emission were systematically investigated. Based on valley and peak ratio of $I_{680.31\text{nm}}/I_{683.03\text{nm}}$ in upconversion emission spectra, temperature sensing with constant absolute sensitivity was achieved. These results suggest $\text{Gd}_2\text{O}_3:\text{Er}^{3+}$ @ $\text{Gd}_2\text{O}_3:\text{Yb}^{3+}$ nanofibers are promising candidates for luminescence thermometry, which may provide their application values in both scientific research and industry.

(Received March 11, 2023; Accepted July 1, 2023)

Keywords: Upconversion, Luminescence thermometry, Core-Shell, Nanofibers, Electrospinning

1. Introduction

Temperature plays a crucial role in both industrial production and scientific research. Diverse traditional methods for temperature sensing such as liquid expansion, thermocouple, thermoresistor, infrared reflection have been used. However, with continued developing of modern industry, these traditional thermometers encounter plenty of challenges included hazardous working environment, biological environment, wide temperature range, motion with high speed, micro-nano scale. Luminescence thermometry based on spectral parameters such as emission intensity, bandshape, position of emission bands, spectral width and luminescence lifetime of

* Corresponding author: liuzhen@jit.edu.cn

nanophosphors has attracted many attentions due to the advantages of high spatial resolution, rapid response and non-invasiveness, which may show great potential in microelectronics and precise medical measurement [1-5]. Therefore, it is of great importance to develop nanophosphors for temperature sensing applications.

Trivalent lanthanide ions play an important role in phosphors due to the abundant energy levels, which can generate emissions ranging from ultraviolet to infrared light through downshifting or upconversion process. In the past decades, a variety of rare earth doped nanophosphors with various sizes and morphologies were developed for sensing, anti-counterfeiting, bio-imaging and lighting. Guo et al. improved the sensing properties of rare earth doped octahedral microcrystals by tuning phonon energy of matrix [6]. Yao et al. construct quantum dots modified $\text{NaYF}_4:\text{Yb}^{3+}, \text{Ho}^{3+}$ nanophosphors for dual-channel anti-counterfeiting ink printing [7], Zhang et al. coded patterns by photon crystal supported luminescent upconversion nanoparticles [8], Choi et al. imaged liver cancer cells via 800 nm excited core-shell-shell upconversion nanoparticles [9], Tian et al. achieved deep tissue imaging by alloyed upconversion nanoparticles [10], Dwivedi et al. reported the color tunable photoluminescence by introducing energy transfer from Ho^{3+} to Eu^{3+} in Y_2O_3 based nanophosphors for potential near-UV excited lighting applications [11]. For upconversion, $\text{Er}^{3+}, \text{Ho}^{3+}, \text{Tm}^{3+}$ ions are widely used as activators and Yb^{3+} ions are generally combined with them for sensitizing due to the large absorption cross-section for near infrared light [12-14].

As another important part of rare earth doped phosphors, host material will provide appropriate sites for the dopants, which are generally sensitizers and activators. The rules for rational selection of host material include small differences in radii between dopant ions and the corresponding substituted ions in host lattice, low phonon energy, physical and chemical stability. The reported host materials include metal organic framework, inorganic fluorides, sulfides and oxides [15-18]. Compared with other three counterparts, oxides have the advantages in thermal and chemical stability. Gd_2O_3 is one type of inorganic oxides, which have low phonon energy. Meanwhile, Gd^{3+} ions have the similar radii with other rare earth ions, making it possible to dope Gd_2O_3 with these ions easily [19]. Hence, it can be anticipated that Gd_2O_3 is an excellent host material for developing inorganic phosphors.

Generally, there have been several methods for fabricating nanophosphors, including hydrothermal synthesis, co-precipitation, combustion, pulsed laser ablation and electrospinning [20-24]. It was worth mentioning that electrospinning technology is a versatile method, which has the advantages in fabricating one-dimensional nanofibers or fiber-like nanocomposites [25, 26]. To the best of our knowledge, although various of metal ions modified Gd_2O_3 nanomaterials have been investigated, there has been little work on the electrospun synthesis of rare earth doped Gd_2O_3 core-shell nanofibers and their photoluminescence.

In this work, the $\text{Gd}_2\text{O}_3:\text{Er}^{3+}@\text{Gd}_2\text{O}_3:\text{Yb}^{3+}$ core-shell nanofibers were fabricated by two-step electrospinning followed by calcination for thermal crystallization. The structural, morphological properties were investigated. The temperature dependent upconversion photoluminescence properties were studied by thermal quenching of emission intensity and thermal induced variations of valley-peak ratios of red emission band.

2. Experimental procedures

$\text{GdN}_3\text{O}_9 \cdot 6\text{H}_2\text{O}$, $\text{ErN}_3\text{O}_9 \cdot 6\text{H}_2\text{O}$, $\text{YbN}_3\text{O}_9 \cdot 5\text{H}_2\text{O}$, N,N-Dimethylformamide (DMF), Polyvinylpyrrolidone (PVP, M_w :1,300,000) were used as raw materials. Before electrospinning, 10 wt% PVP was dissolved in DMF to obtain solution. After that, the stoichiometric $\text{GdN}_3\text{O}_9 \cdot 6\text{H}_2\text{O}$ and $\text{ErN}_3\text{O}_9 \cdot 6\text{H}_2\text{O}$ were blended in the PVP solution with stirring to get the Er^{3+} , Gd^{3+} precursor solution. The Yb^{3+} , Gd^{3+} precursor solution was prepared by the similar process. In the first round electrospinning process, the Er^{3+} , Gd^{3+} polymer precursor solution was introduced in 10 mL syringe and electrospun by adding a voltage of 15 KV between the 0.2 mm stainless steel needle of syringe and the aluminum foil attaching on rotated collector. The distance of needle and collector was fixed at 12 cm and the flow rate of precursor solution was 0.5 mL/h. After the electrospinning, the PVP film contained Er^{3+} and Gd^{3+} was peeled from the aluminum foil and followed by calcined at 700 °C in the muffle furnace.

For coating a sensitized shell on the active core nanofibers obtained from the first electrospinning and calcining. The inorganic powders were weight and ultrasonic dispersed in Yb^{3+} , Gd^{3+} precursor solution. The resultant precursor solution were electrospun on aluminum foil as the process in the first round electrospinning. Finally, the composite films were calcined in the muffle furnace at 700 °C for 1 h to burn out organic components and crystallize the nanocomposites.

The structural information of core-shell nanofibers was characterized by X-Ray diffraction (D/max 2400, Rigaku Corp., Cu-K α radiation, $\lambda=1.5406\text{\AA}$). The surface morphology of powders was recorded by scanning electron microscope (Quanta 250 FEG). The 980 nm diode laser with tunable power ranging from 0 to 1 W was used as excitation light source. The upconversion photoluminescence spectra of nanofibers at various temperatures were collected via a fiber optic spectrometer (PG2000 Pro, Ideaoptics, China). Temperature control stage has a precision of 0.1 °C.

3. Results and discussion

Fig. 1 shows the X-Ray diffraction pattern of the synthesized core-shell $\text{Gd}_2\text{O}_3:\text{Er}^{3+}$ @ $\text{Gd}_2\text{O}_3:\text{Yb}^{3+}$ nanofibers in the diffraction angle (2θ) range from 10° to 60°. It is clear to see that the pattern have several intense diffraction peaks, which appeared at 20.2°, 28.8°, 33.3°, 47.8° and 56.6°, respectively. These peaks can be indexed to the (211), (222), (400), (440) and (622) crystal planes, which can be matched well with standard PDF card (No.12-0797) of cubic phased Gd_2O_3 . No impurity phase illustrates the Er^{3+} and Yb^{3+} ions are substituted into Gd_2O_3 host matrix and the core-shell structure have no phase change resulted from the same matrix material for core and shell.

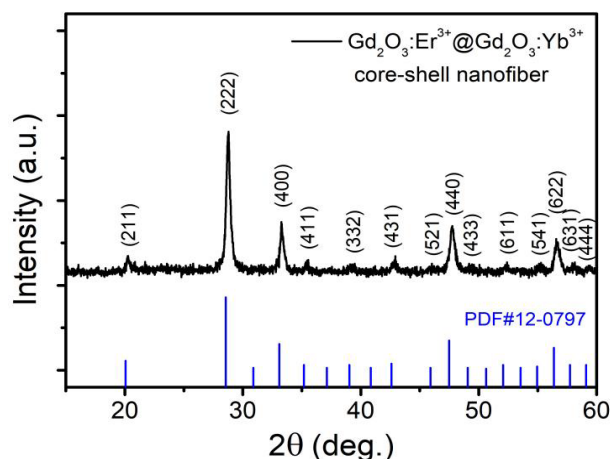


Fig. 1. X-Ray diffraction patterns of electrospun $Gd_2O_3:Er^{3+}@Gd_2O_3:Yb^{3+}$ nanofibers.

The surface morphological image of composite nanophosphors obtained via scanning electron microscopy (SEM) are displayed in Fig. 2(a). As can be seen from the image, the nanofibers exhibit core-shell structure with the cross sectional diameter less than $1\mu m$. Furthermore, Fig. 2(b) displays the surface morphology of the nanofibers along the longitudinal direction. It can be clearly observed that synthesized nanofibers have the rough tree bark-like surface, which is due to the aggregation of plenty of ultrafine $Gd_2O_3:Yb^{3+}$ nanoparticles in the process of shell formation.

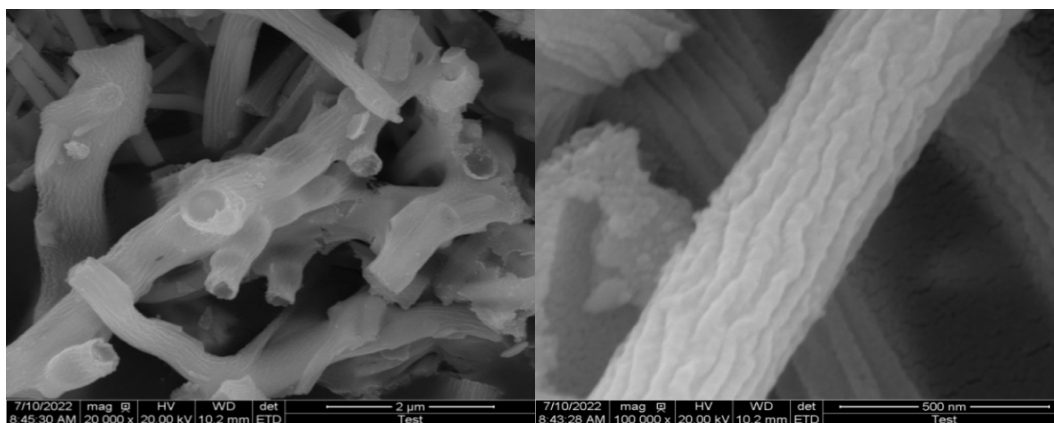


Fig. 2. Morphological image of electrospun $Gd_2O_3:Er^{3+}@Gd_2O_3:Yb^{3+}$ nanofibers

As the important active ions for upconversion photoluminescence, under the near-infrared light excitation, Er^{3+} ions can exhibit visible emission, which is attributed the characteristic transitions from coupled excited state ($^2H_{11/2}, ^4S_{3/2}$) to ground state $^4I_{15/2}$ and excited state $^4F_{9/2}$ to ground state $^4I_{15/2}$. For further enhancing the absorption cross-section of near-infrared excited light, Yb^{3+} ions are generally combined with active ions for sensitizing. According to the previous reports, the strong red emission can be achieved by doping high concentration of Yb^{3+} ions [27].

The temperature dependent upconversion photoluminescence emission spectra with range from 400 nm to 750 nm in the temperature range from 303 K to 543 K are shown in Fig. 3 . It can be observed that red emission band is stronger than green emission band at each temperature, which can be attributed the heavy doping of Yb^{3+} in shell and the energy reverse transfer from Er^{3+} ions in core to the Yb^{3+} ions in shell. The strong red emission band has three peaks, which are resulted from stark splitting of energy levels induced by crystal field. In addition, the peak positions in photoluminescence emission spectra are hardly changed with temperature for the nanofibers. However, the intensity of red emission shows obvious dependence of temperature. As the elevation of temperature, the intensity of red emission drastically decrease due to thermal quenching. For clearly observing the corresponding variation of green emission as the temperature increases, Fig. 4 displays the enlarged diagram of weak green emission band in the range from 500 nm to 600 nm. The intensity of peak situated at 562 nm decreases with increasement of temperature, while the intensity of peak around 525 nm changes little. The result is coincided with the thermal coupled energy assisted energy population.

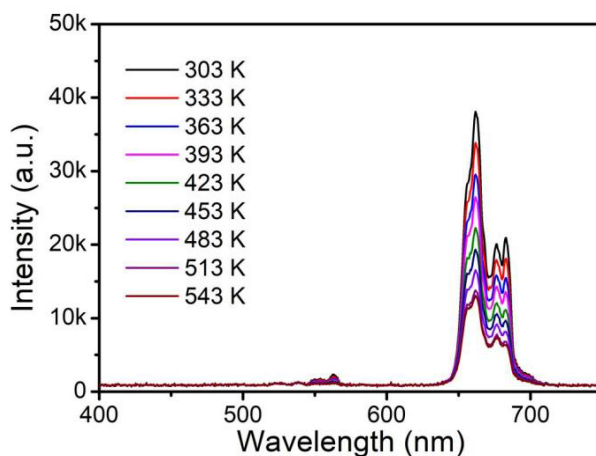


Fig. 3. Temperature dependent visible upconversion emission spectra of $\text{Gd}_2\text{O}_3:\text{Er}^{3+}@\text{Gd}_2\text{O}_3:\text{Yb}^{3+}$ core-shell nanofibers under 980 nm excitation.

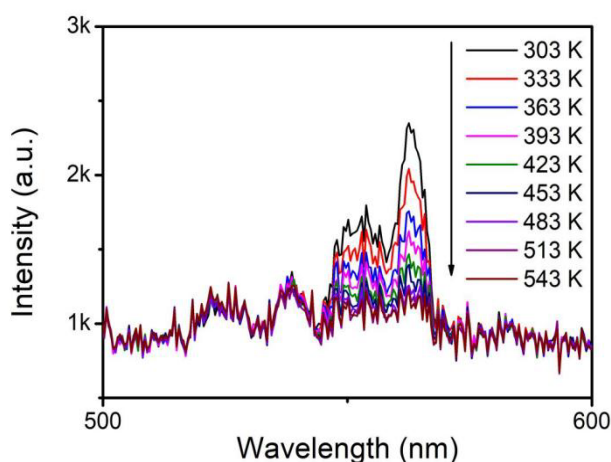


Fig. 4. Green emission band of $\text{Gd}_2\text{O}_3:\text{Er}^{3+}@\text{Gd}_2\text{O}_3:\text{Yb}^{3+}$ core-shell nanofibers as a function of temperature.

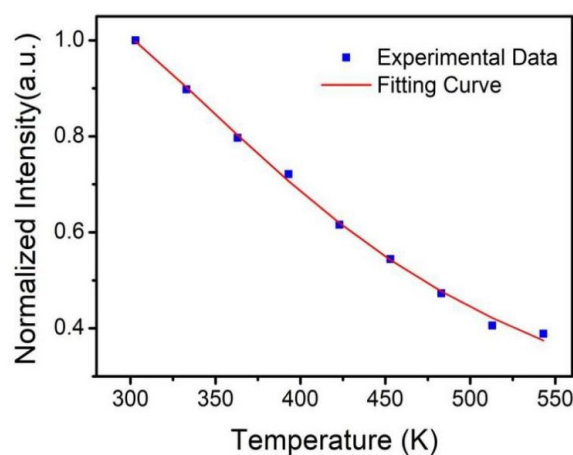


Fig. 5. Normalized integral intensity of red emitting band as a function of temperature.

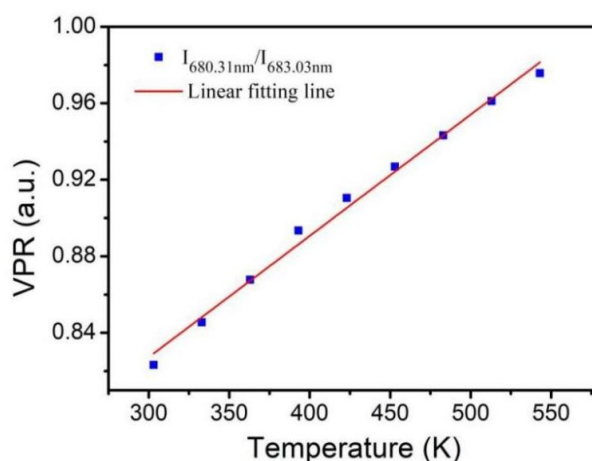


Fig. 6. Valley and peak ratios at different temperature.

For further investigating the thermal induced quenching behavior of red emitting band, the normalized integral intensity of red emission of the core-shell nanofibers as a function of temperature are marked as the blue square dots in Fig. 5. As shown, the intensity at 543 K is decreased 60% more than that at initial temperature. According to thermal quenching theory, the temperature dependent luminescence intensity can be quantitative described as following equation (1) [28].

$$I(T) = \frac{I_0}{1 + Ae^{-\frac{\Delta E}{kT}}} \quad (1)$$

where I_0 represents the intensity at 0 K, A is a constant, k is Boltzmann constant, T is the absolute temperature, ΔE is the activation energy in thermal quenching process. The fitting result is shown by the red line in Fig. 5. According to the fitting calculation, ΔE is equal to 0.1408, indicating the thermal quenching can be easily activated and the luminescence is sensitive to variation of temperature.

The fluorescence intensity ratio technique based on valley and peak ratio (VPR) was introduced to further describe the optical temperature sensing characteristics of the synthesized nanofibers. Fluorescence intensity of the right valleys and peaks at different temperature were selected for calculating VPR. Fig. 6 displays the experimental data of VPR of $I_{680.31\text{nm}}$ and $I_{683.03\text{nm}}$ as a function of temperature. As shown in the figure, VPR ($I_{680.31\text{nm}}/I_{683.03\text{nm}}$) is increased as raising temperature. The values varied from 0.82 at 303 K to 0.98 at 543 K with a growth rate of 19%. For quantitative analysis, the data was fitting by a linear function, which is advantageous for practical applications in temperature sensing due to its constant absolute sensitivity. This can be explained by the definition of absolute sensitivity (S_a), which can be expressed as following equation (2).

$$S_a = \left| \frac{dVPR}{dT} \right| \quad (2)$$

As shown in Fig. 6, the experimental data can be fitted by a straight line, which is marked red. The linear fitting function of the temperature dependent VPR ($I_{680.31\text{nm}}/I_{683.03\text{nm}}$) in the temperature range from 303 K to 543 K can be written as the equation (3).

$$VPR = 0.000634 * T + 0.63704 \quad (3)$$

Another important index for temperature sensing is relative sensitivity (S_r), which can be calculated by following equation (4).

$$S_r = \left| \frac{1}{VPR} \frac{dVPR}{dT} \right| * 100\% \quad (4)$$

It can be calculated that S_r has its maximum value of $0.07\% \text{ K}^{-1}$ at 303 K in measured temperature range for the synthesized $\text{Gd}_2\text{O}_3:\text{Er}^{3+}@\text{Gd}_2\text{O}_3:\text{Yb}^{3+}$ core-shell nanofibers.

4. Conclusion

In conclusion, $\text{Gd}_2\text{O}_3:\text{Er}^{3+}@\text{Gd}_2\text{O}_3:\text{Yb}^{3+}$ core-shell nanofibers were developed by electrospinning followed by calcination. Under 980 nm near-infrared light excitation, the strong red emission and weak green emission were obtained in visible wavelength range. The strong red emission band include three peaks due to stark splitting of energy level. The upconversion photoluminescence of synthesized nanofibers were sensitive to variation of temperature. The thermal quenching behavior of red emission was investigated. The activation energy for thermal quenching was 0.1408 eV. VPR ($I_{680.31\text{nm}}/I_{683.03\text{nm}}$) as a function of temperature can be described as a linear function. All the results suggest the $\text{Gd}_2\text{O}_3:\text{Er}^{3+}@\text{Gd}_2\text{O}_3:\text{Yb}^{3+}$ core-shell nanofibers have great potential for temperature sensing based on upconversion photoluminescence.

Acknowledgements

This work is financially supported by the Research Start-up Program of Jinling Institute of Technology (jit-b-202054), Jiangsu Province's Double Innovation Plan (JSSCBS20210616), National Natural Science Foundation of China (Grant No.11804150), Natural Science Foundation of Jiangsu Province (BK2020111), Entrepreneurship Training Program for College Students of Jiangsu Province (202213573110Y).

References

- [1] Z. Liu, G. C. Jiang, R. X. Wang, C. K. Chai, L. M. Zheng, Z.G.Zhang, B.Yang, W.W.Cao, *Ceramics International* 42, 11309 (2016)
- [2] R. G. Geitenbeek, J. C. Vollenbroek, H. M. H. Weijgertze, C. B. M. Tregouet, A. Nieuwelink, C. L. Kennedy, B. M. Weckhuysen, D. Lohse, A. V. Blaaderen, A. V. D. Berg, M. Odijk, A. Meijerink, *Lab on a Chip* 19, 1236 (2019); <https://doi.org/10.1039/C8LC01292J>
- [3] Z. Liu, R. X. Wang, *Chalcogenide Letters* 19, 471 (2022); <https://doi.org/10.15251/CL.2022.197.471>
- [4] A. S. Laia, D. A. Hora, M. V. S. Rezende, Y. T. Xing, J. J. Rodrigues Jr, G. S. Maciel, M. A. R. C. Alencar, *Journal of Luminescence* 227, 117524 (2020); <https://doi.org/10.1016/j.jlumin.2020.117524>
- [5] Z. Liu, R. X. Wang, D. H. Chen, *Journal of Materials Science: Materials in Electronics* 33, 3748 (2022); <https://doi.org/10.1007/s10854-021-07566-y>
- [6] J. K. Yao, G. L. Pena, J. Lifante, M. C. Cruz, R. Marin, E. M. Rodriguez, D. Jaque, D. H. Ortgies, *Optical Materials: X* 17, 100225 (2023); <https://doi.org/10.1016/j.omx.2022.100225>
- [7] Q. Yao, H. Y. Wu, Y. H. Jin, C. L. Wang, R. T. Zhang, Y. H. Hu, *Journal of Luminescence* 251, 119186 (2022); <https://doi.org/10.1016/j.jlumin.2022.119186>
- [8] H. B. Zhang, L. L. Xu, F. C. Liu, C. Huang, J. Wei, *Nanotechnology* 30, 505706 (2019); <https://doi.org/10.1088/1361-6528/ab4244>
- [9] J. E. Choi, H. W. Kim, Y. S. Kim, G. Y. Kim, T. S. Lee, S. H. Kim, D. H. Kim, H. S. Jang, *Materials and Design* 195, 108941 (2020); <https://doi.org/10.1016/j.matdes.2020.108941>
- [10] B. Tian, A. Fernandez-Bravo, H. Najafiaghdam, N. A. Torquato, M. V. P. Altoe, A. Teitelboim, C.A. Tajon, Y. Tian, N. J. Borys, E. S. Barnard, M. Anwar, E. M. Chan, P. J. Schuck, B. E. Cohen, *Nature Communication* 9, 3082 (2018); <https://doi.org/10.1038/s41467-018-05577-8>
- [11] A. Dwivedi, M. Srivastava, A. Srivastava, C. Upadhyay, S. K. Srivastava, *Scientific Reports* 12, 5824 (2022)
- [12] Zhang, X. C. Yu, X. Q. Xue, B. Y. Gao, Y. R. Bai, H. B. Yang, X. J. Li, J. B. Fan, P. Zhao, *Journal of Alloys and Compounds* 930, 167357 (2023); <https://doi.org/10.1016/j.jallcom.2022.167357>
- [13] S. F. Liu, J. Cui, J. J. Jia, J. X. Fu, W. X. You, Q. Y. Zeng, Y. M. Yang, X. Y. Ye, *Ceramics International* 45, 1 (2019)
- [14] H. Q. Yu, P. P. Jiang, B. J. Chen, J. S. Sun, L. H. Cheng, X. P. Li, J. S. Zhang, Sai Xu, *Applied Physics A* 126, 690 (2020)

- [15] W. Liu, M. Y. Zhao, G. T. Xiang, Z. L. Han, F. Xia, J. W. Wang, *Journal of Luminescence* 239, 118296 (2021); <https://doi.org/10.1016/j.jlumin.2021.118296>
- [16] D. Przybylska, T. Grzyb, *Journal of Alloys and Compounds* 831, 154797 (2020); <https://doi.org/10.1016/j.jallcom.2020.154797>
- [17] M. M. Lun, W. Y. Wu, Z. F. Xing, H. Z. Song, Y. Z. Wang, W. Li, B. L. Chu, Q. Y. He, *Journal of Luminescence* 223, 117189 (2020); <https://doi.org/10.1016/j.jlumin.2020.117189>
- [18] C. D. Zuo, W. Tang, C. Y. Ma, C. Chang, K. F. Fan, Y. K. Li, X. Y. Yuan, Z. C. Wen, Y. G. Cao, *Journal of Luminescence* 255 119585 (2023); <https://doi.org/10.1016/j.jlumin.2022.119585>
- [19] S. Nambram, S. D. Singh, *Materials Today: Proceedings* 65, 2520 (2022); <https://doi.org/10.1016/j.matpr.2022.04.508>
- [20] Z. Yuan, C. Shen, Y. L. Zhu, A. Q. Bai, J. Wang, Y. F. Liun, Y. N. Lyu, *Ceramics International* 42, 1513 (2016); <https://doi.org/10.1016/j.ceramint.2015.09.099>
- [21] Y. Tian, F. Lu, M. M. Xing, J. C. Ran, Y. Fu, Y. Peng, X. X. Luo, *Optical Materials* 64, 58 (2017); <https://doi.org/10.1016/j.optmat.2016.11.031>
- [22] H. Ahmadian, F. A. Hessari, A. M. Arabi, *Ceramics International* 45, 18778 (2019); <https://doi.org/10.1016/j.ceramint.2019.06.106>
- [23] H. W. Deng, J. Liu, H. Zhang, C. R. Li, Z. Liu, D. H. Chen, *Journal of Materials Science: Materials in Electronics* 32, 14932 (2021); <https://doi.org/10.1007/s10854-021-06045-8>
- [24] H. Q. Yu, Y. Li, Y. Song, Y. B. Wu, B. J. Chen, P. Li, *Ceramics International* 42, 1307 (2016); <https://doi.org/10.1016/j.ceramint.2015.09.066>
- [25] M. M. Xu, W. Y. Ge, J. D. Shi, Y. X. Li, *Journal of Alloys and Compounds* 861, 158622 (2021); <https://doi.org/10.1016/j.jallcom.2021.158622>
- [26] Z. L. Gao, Y. Li, E. Y. B. Pun, H. Lin, *Dyes and Pigments* 194, 109645 (2021); <https://doi.org/10.1016/j.dyepig.2021.109645>
- [27] J. Liu, H. W. Deng, Z. Y. Huang, Y. L. Zhang, D. H. Chen, Y. Z. Shao, *Physical Chemistry Chemical Physics* 17, 15412 (2015); <https://doi.org/10.1039/C5CP01632K>
- [28] Z. Liu, H.W. Deng, D.H. Chen, *Ceramics International* 45, 13235 (2019); <https://doi.org/10.1016/j.ceramint.2019.04.009>